

Computer simulation of temperature distribution on a solid target for ^{201}Tl production

Mohammad R. Aboudzadeh Rovais,
Kamran Yousefi,
Khosro Ardaneh,
Mohammad Mirzaii

Abstract. Thallium-201 is of great interest in nuclear medicine for diagnostic purposes. It is produced by the $^{203}\text{Tl}(p,3n)^{201}\text{Pb}$ nuclear reaction. Since the target for ^{201}Tl production is a solid target and the maximum beam current for the irradiation has a direct relation with its temperature surface, therefore, the control of temperature during the irradiation is essential. Designing a proper cooling system is one of the important and determining parameters in radionuclide production efficiency. Non-controlled temperature would cause melting and consequently loss of target materials that could be very costly especially when an isotopically enriched material is used. In this study, the heat transfer and temperature distribution on the target has been simulated based on a computational fluid dynamics (CDF) code for the thermal behavior of the target during the irradiation and under the different beam currents, cooling flow rates and target designing. The results on the routinely used target for the production of ^{201}Tl in AMIRS, showed that there was a good linearity between proton beam currents (in the range of 100–350 μA) and maximum temperature on the thallium target (345–458 K). The results also showed that the flow rate of the cooling water can be brought down (from routinely used 45 L/min) to 15 L/min without any risk of melting of target material.

Key words: heat transfer • computer simulation • solid target • thallium-201

Introduction

$^{201}\text{TlCl}$ is one of the most important cyclotron products being used in nuclear medicine for diagnostic purposes such as myocardial imaging [6, 8]. However, non cardiac applications have been reported [2–5, 10, 12].

The radionuclide ^{201}Tl is produced by proton-irradiation of an enriched ^{203}Tl target in a cyclotron involving the nuclear reaction $^{203}\text{Tl}(p,3n)^{201}\text{Pb}$ followed by the decay of the parent nuclide ^{201}Pb ($T_{1/2} = 9.33$ h) into ^{201}Tl ($T_{1/2} = 76.03$ h) by electron capture.

Solid targets for production of many radionuclides by proton beams have played a great role in nuclear medicine. The mass production of ^{201}Tl often employs a solid target system, where enriched ^{203}Tl metal is electrodeposited onto a copper backing plate. For production of the radionuclide, the metallic solid target is irradiated by energetic protons (28.5 MeV) produced in a cyclotron which can produce beam currents of several hundred microamperes. Although production yields can be enhanced by increasing the proton beam current, the maximum beam deposited on a target is limited by the targetry including thermal characteristics of the target material and cooling system to prevent possible loss of the target material. Thus, it is required to investigate the optimal operating condition of the solid target to obtain high production rate of ^{201}Tl . Since the demand for ^{201}Tl from nuclear medicine centers in the country has been increasingly grown, the main objective of this

M. R. Aboudzadeh Rovais✉, K. Yousefi, K. Ardaneh,
M. Mirzaii
Agricultural, Medical and Industrial Research School
(AMIRS),
Nuclear Science and Technology Research Institute
(NSTRI),
P. O. Box 31485-498, Karaj, Iran,
Tel.: +98 261 441 1101, Fax: +98 261 441 1106,
E-mail: mraboudzadeh@nrcam.org

Received: 2 December 2010

Accepted: 20 June 2011

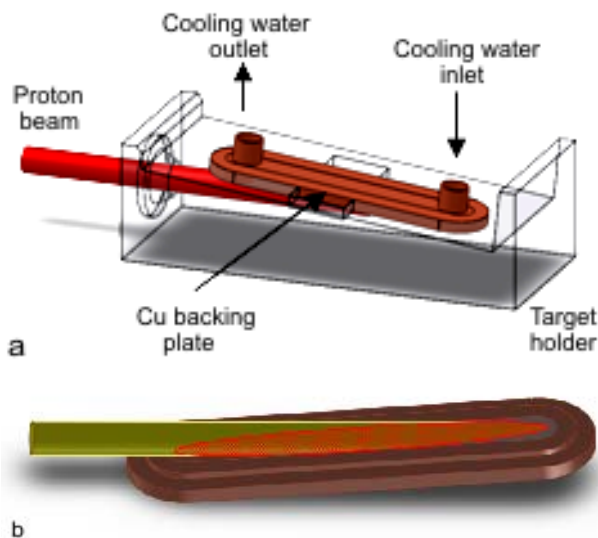


Fig. 1. The existing solid target system in AMIRS: (a) target system and (b) an inclined plane target used for irradiation of solid materials.

study was to investigate how to possibly increase the proton beam currents and the productivity of ²⁰¹Tl.

Methods

In the Nuclear Medicine Research Group that belongs to the Nuclear Science and Technology Research Institute, the Atomic Energy Organization of Iran has installed a cyclotron Cyclon-30 (manufactured by IBA, Belgium) which accelerates H⁻ ions and extracts H⁺ ions with variable energy between 15–30 MeV and beam current up to 350 μA.

One of the difficult problems in accelerator targetry is dissipation of the heat generated as the beam passes through the matter. One approach, often taken with solid targets, is to use an angle of α inclined plane to spread the beam out over a large area and thereby reduce the power density in the striking beam area. An example of this type of target system, which has been used routinely in AMIRS, is shown in Fig. 1.

The solid target is a thin layer of thallium electrodeposited onto a copper plate. At the rear of the copper plate, there is a cooling water to transfer heat convectively. Copper was chosen because it is relatively easy to electroplate thallium onto it and has an excellent thermal conductivity, which is important for removal of heat from the thallium. Some important properties of Cu and Tl are listed in Table 1.

Thallium has low thermal conductivity (0.46 W·cm⁻¹·K⁻¹); therefore, the most critical issue in the design of a production target is to provide an effective cooling system in order to avoid melting of the thallium layer. In addition, its solid vapor pressure increases logarithmically with temperature as shown in

Table 1. Important properties of copper and thallium

Element	Density (g·cm ⁻³)	Melting point (°C)	Thermal conductivity (W·cm ⁻¹ ·K ⁻¹)	Specific heat (J·kg ⁻¹ ·°C ⁻¹)
Copper	8.96	1083	4.03	384
Thallium	11.85	303	0.46	130

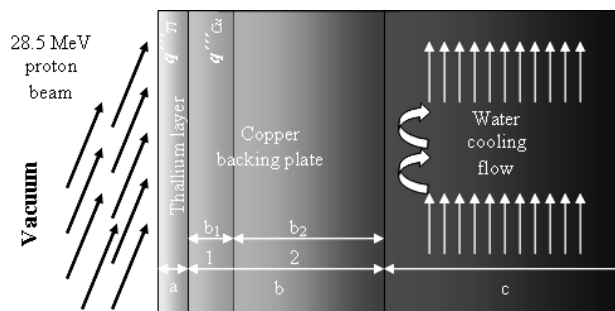


Fig. 2. The three layers of the thallium target.

Eq. (1) [9] and, as a result, some of the expensive target material might be lost if the cooling is not efficient. Thus, the optimization of the cooling system is of utmost importance for achieving cost effective production.

$$(1) \quad \log(p) = 10.977 - 9447/T$$

In this equation *p* is in Pascals and *T* in K.

Tl target can be considered as a three-layer system, facing the accelerator vacuum on one side and the cooling water on the other side as shows in Fig. 2.

Layer 1 in Fig. 2 is the ²⁰³Tl deposit denoted by *a* cm. In this layer, ²⁰¹Pb is produced by the ²⁰³Tl(p,3n)²⁰¹Pb nuclear reaction at a beam-target angle of α. The energy loss of protons in this layer is converted to heat (*q''_{Tl}*).

Layer 2, the Cu-1 layer, has a physical thickness of *b*₁ cm. In this layer, protons emerging from the thallium layer are stopped completely. The *q''_{Cu}* is heat generated in this layer.

Layer 3, the Cu-2 layer, has a physical thickness of *b*₂ cm and serves as a mechanical support for the thallium layer. The total heat (*q''_T*) produced in the layers *q''_{Tl}* and *q''_{Cu}* is transferred to the cooling water through this layer by conduction:

$$(2) \quad q''_T = q''_{Tl} + q''_{Cu}$$

As mentioned before, the interaction of energetic proton beam with matter generates a relatively high density of heat. The heat generated in each layer by the energetic proton beam with kinetic energy *E* (MeV) and beam current *I* (μA) is expressed by the equation:

$$(3) \quad q''' \text{ (watt)} = E \times I$$

Conductive and convective heat transfer was modeled using the general heat transfer application as follows. The heat transfer by conduction is governed by the law of conservation of thermal energy for solids and incompressible fluids as [1]:

$$(4) \quad \rho c \frac{dT}{dt} + \nabla \cdot q = q'''$$

where: ρ is the density (g·cm⁻³); *c* is the heat capacity

(J·cm⁻³·K⁻¹); T is the temperature (K); k is the thermal conductivity (W·cm⁻¹·K⁻¹); q is the heat transfer (W·cm⁻²). The Fourier's law for homogeneous continua is:

$$(5) \quad q = -k \nabla T$$

Inserting Eq. (5) into Eq. (4) gives:

$$(6) \quad \frac{dT}{dt} = \psi \nabla^2 T + \frac{q''}{\rho c}$$

where

$$(7) \quad \psi = k / \rho c$$

A model of the target configuration is divided into a number of layers with small elements which are usually with a brick shape defined as nodes. The temperature at each node is then calculated, taking into account the thermal conductivity of material and the thermal boundary conditions (heat regions and cooled surface) imposed on the target. The encountered boundary conditions in this system are:

- a) No heat flux (insulation) on the surface of thallium layer ($(\partial T_a / \partial n) = 0$ where $\partial / \partial n$ denotes differentiation along the normal of boundary).
- b) Heat flux at the interface of two continua (thallium and copper) with different conductivities [$k_{Tl}(\partial T_a / \partial n) = k_{Cu}(\partial T_{b_1} / \partial n)$].
- c) Heat transfer of the copper backing to the cooling water by convection [$-k_{Cu}(\partial T_{b_2} / \partial n) = h(T_s - T_{water})$], where T_s and T_{water} are the surface temperature of the Cu backing and the cooling water temperature, respectively).

Forced convective heat transfer boundary conditions were applied to the copper backing facing the cooling channel surfaces. Cooling was assumed to be uniform along the channels. The Dittius-Boelter formulation was used to calculate the convection coefficient by the Nusselt number ($Nu = (hD/k)$) as the ratio of convection heat transfer to conduction heat transfer [7, 11, 13].

$$(8) \quad Nu = 0.023 \times Re^{0.8} \times Pr^{0.4}$$

where Reynolds number ($Re = (\rho u D / \mu)$) represents the ratio of the inertial force of the fluid to the viscous forces of the fluid and the Prandtl number ($Pr = (\mu C / k)$) represents the ratio of the viscous properties of the fluid to the heat transfer properties. D and μ are hydraulic diameter (cm) and dynamic viscosity (cm²·s⁻¹). This equation is valid for water in circular pipes with the turbulent range of $10\,000 \leq Re \leq 160\,000$. However, this equation can be used in non-circular pipes using the proper hydraulic diameter [7]. The hydraulic diameter is given by:

$$(9) \quad D = \frac{4 \times (\text{cross sectional area of flow})}{\text{wetted perimeter}}$$

Results and discussion

The SolidWorks® 2010 was used to simulate the target by considering the basic model equations explained earlier. The simulator solves the governing equation with the finite volume (FV) method on a spatially rectangular computation mesh designed in the Cartesian coordination system. In this analysis, the different layers were modeled in steady state of the thermal responses of the target to the beam heating and cooling conditions.

In this study, the thallium target was irradiated with proton beams at an angle of $\alpha = 6^\circ$ on the Cu backing plate ($b = 1$ mm). The kinetic energies of 28.5 MeV protons are lost as they pass through the target material. At this angle, basing on the results of SRIM code, the vertical depth needed to degrade 28.5 MeV protons to 20 MeV in the thallium layer and degrading 20 MeV protons to 0 MeV in the copper backing was calculated to be $a = 76 \mu\text{m}$ and $b_1 = 84 \mu\text{m}$, respectively. The SRIM code calculates the stopping power and range of ions (10 eV – 2 GeV/amu) into matter using a full quantum mechanical treatment of ion-atom collisions [14]. The heat generated at the different layers was also estimated by SRIM code. Figure 3 shows the simulated stopping ranges for protons in the energy range of 10–30 MeV on thallium and copper.

In this modeling, it was assumed that the cyclotron beam profile was uniform and has a diameter of 1 cm. Since the heat generation in each layer (Eq. (2)) is a function of the beam current, in each layer it was calculated for different proton beam currents. The results are shown in Table 2.

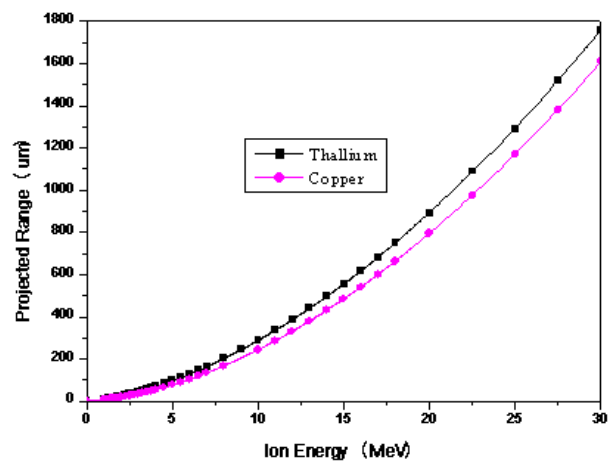


Fig. 3. Projected range of proton on thallium and copper.

Table 2. Heat generation in different layers at different proton beam currents

I (μA)	q'' (W)		
	Thallium (28.5–20 MeV)	Copper 1 (20–0 MeV)	Total power deposited in the target
100	850	2000	2850
200	1700	4000	5700
250	2125	5000	7125
300	2550	6000	8550
350	2975	7000	9975

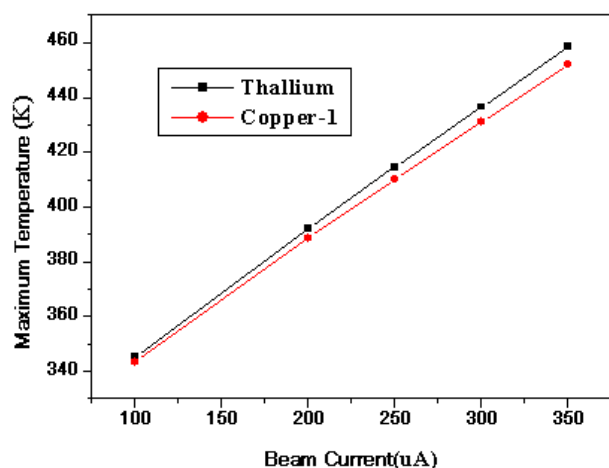


Fig. 4. The maximum temperature on the thallium and copper layers in the range of 100–350 μA of 28.5 MeV proton beam.

The temperature of the thallium, copper and outlet water at the different beam currents are listed in Table 3 where the cooling water temperature and flow rate are fixed on 293 K and 45 L/min, respectively.

It can be seen in Fig. 4 that there is almost a linear relation between the maximum temperature on thallium

Table 3. Maximum temperatures of thallium, copper and outlet water on different beam currents irradiation

I (μA)	T (K)		
	Thallium	Copper 1	Outlet cooling water
100	345	343	294
200	392	389	295
250	415	410	296
300	436	431	296
350	458	452	297

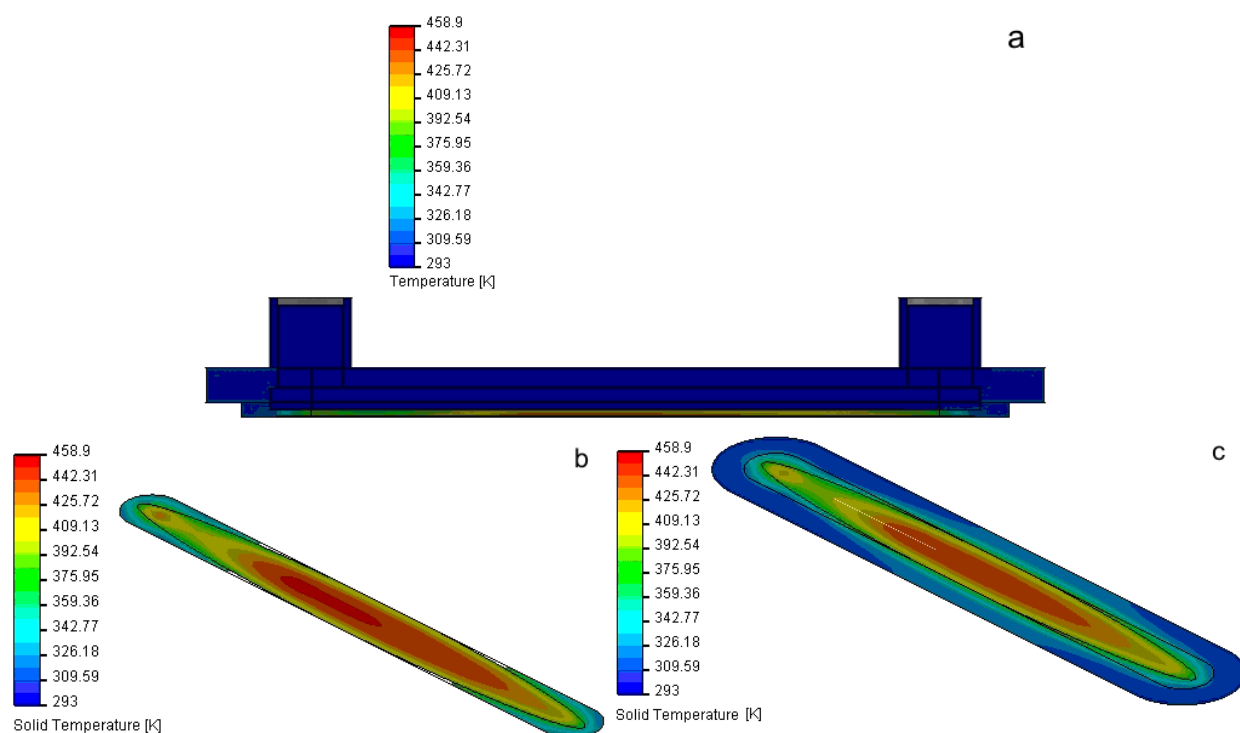


Fig. 5. Simulation results for the temperature distribution in (a) the target assemble, (b) the thallium and (c) the copper ($T_{\text{water}} = 293$ K).

and copper layers and beam currents in the range of 100–350 μA . The maximum temperature at the thallium surface under the beam current of 350 μA is less than its melting point (577 K).

The modeled temperature distribution on the layers of thallium and copper are shown in Fig. 5, where the target is irradiated with the 28.5 MeV proton beam at a current of 350 μA and a flow water rate of 45 L/min.

It can be seen in Fig. 5 that the maximum temperature of the target is located at the middle of the target due to higher density of heat generation and it is still lower than the thallium melting point. Therefore, the existing cooling system has extra power to remove the generated heat and prevent melting of thallium.

In this study, the maximum temperatures of thallium with the water flow rates of 10, 15, 25, 35 and 45 L/min at the fixed proton energy (28.5 MeV) and beam current (350 μA) were investigated. As shown in Fig. 6, thallium is melted if the flow rate is 10 L/min. The optimum water flow rate for irradiation of thallium target was, therefore, considered to be about 15 L/min.

There is an interesting point in Fig. 6a where this is depicted. In this simulation, there is an inhomogeneous temperature distribution on the left side of the thallium layer. To explain this phenomenon, it is better to look at the simulated water velocity in the cooling channel of the

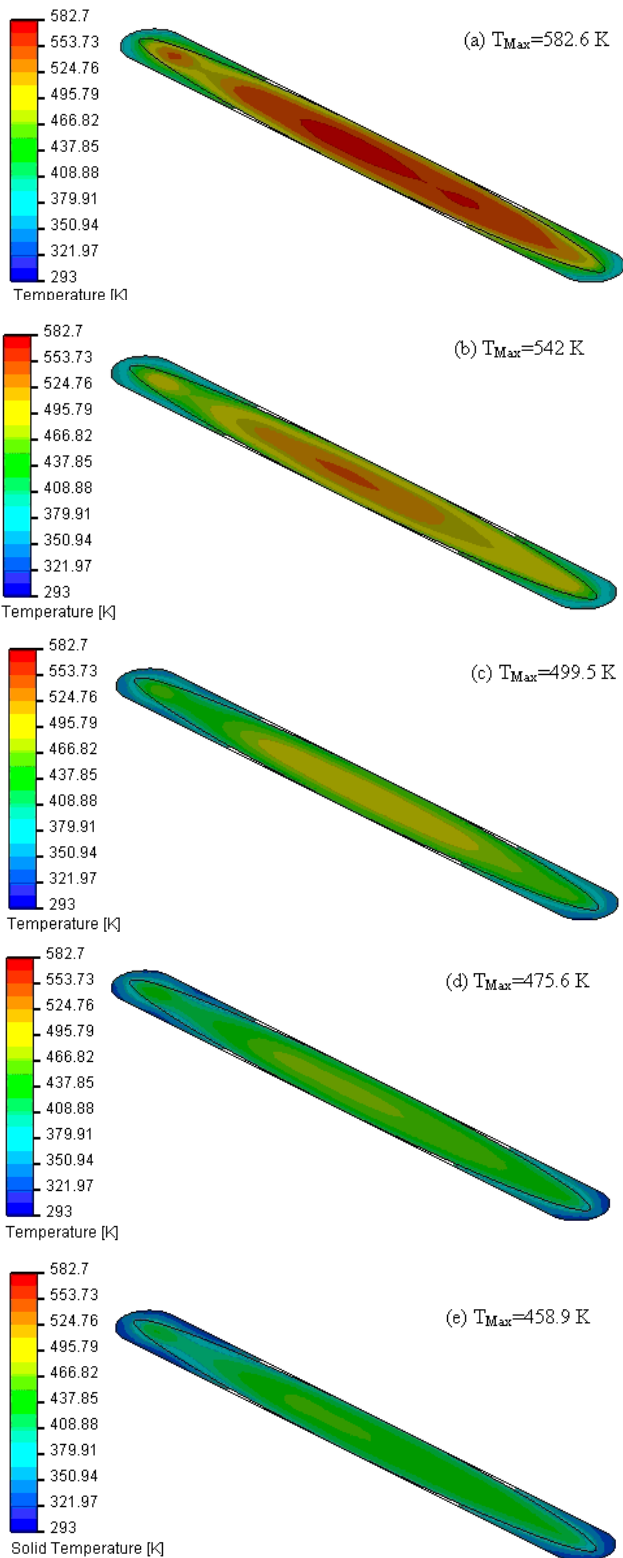


Fig. 6. The modeled thallium temperature distribution with the cooling water ($T_{\text{water}} = 293 \text{ K}$) at flow rates (a) 10 L/min ($Re = 27\,800$), (b) 15 L/min ($Re = 45\,255$), (c) 25 L/min ($Re = 74\,348$), (d) 35 L/min ($Re = 105\,380$) and (e) 45 L/min ($Re = 140\,938$).

target system (Fig. 7a). It can be found the water velocity is reduced quickly due to suddenly changed direction of water, while if this changed direction is happened at a more moderate angle, by considering a bending surface ($r = 25 \text{ mm}$) on the inlet area, then the water velocity

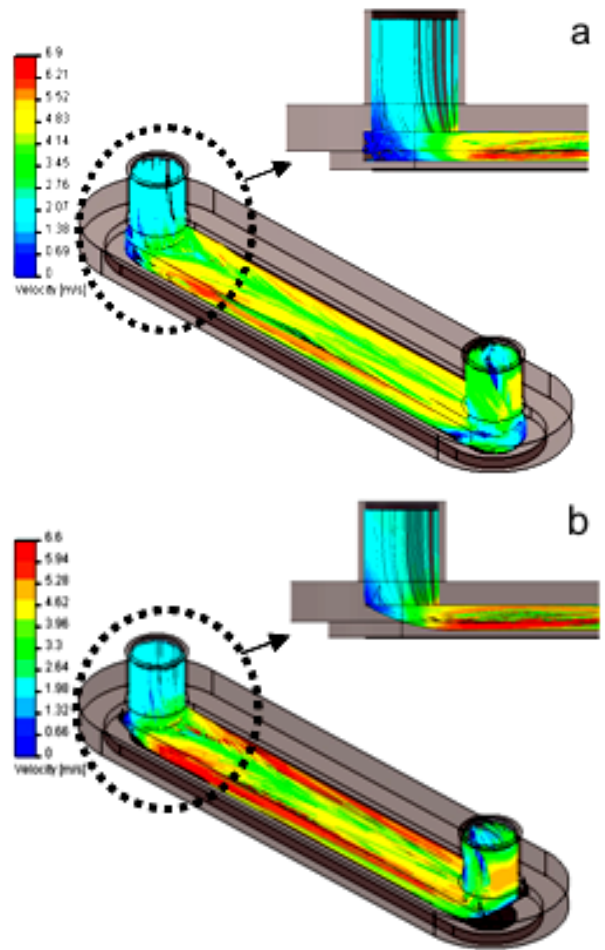


Fig. 7. Simulation of water velocity in the cooling channel (a) with right angle inlet and (b) with moderately curved inlet ($T_{\text{water}} = 293 \text{ K}$).

can be less decreased (Fig. 7b) and consequently the heat transfer coefficient will be higher in this area (see Eq. (7)). As shown in Fig. 8, the considered non homogeneous area has been weakened by this modification.

As explained before, the forced convective heat transfer boundary conditions were applied on the copper backing facing the cooling channel surfaces. The convection heat transfer ($q_{\text{convection}}$) may be increased by increasing: (i) the temperature difference between the wall and cooling water (ΔT); (ii) the heat transfer coefficient (h), or (iii) the heat transfer area (A) as shown in Eq. (10).

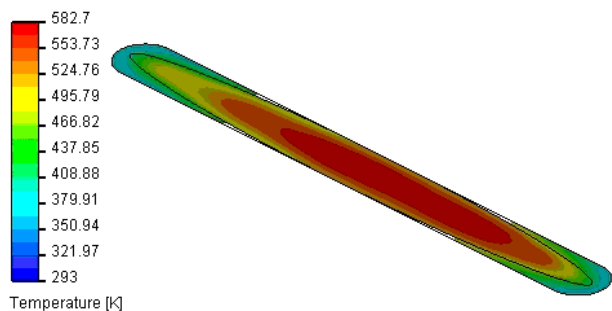


Fig. 8. The simulated temperature distribution in the thallium layer with cooling water at flow rate of 10 L/min when there is a bending surface in rear surface of copper plate ($T_{\text{water}} = 293 \text{ K}$).

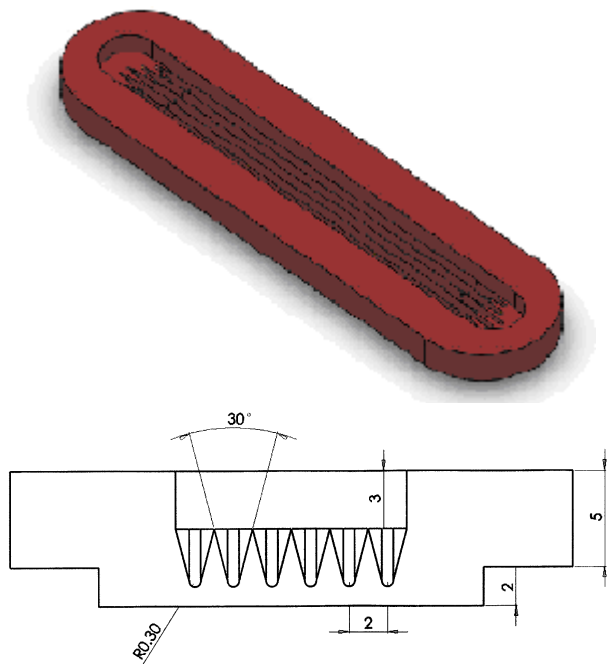


Fig. 9. The target copper backing with fins and its cross sectional dimensions.

$$(10) \quad q_{\text{convection}} = h \cdot A \cdot \Delta T$$

One of the objectives of this study was to improve the convective heat transfer by using the extended surfaces or fins. The copper backing with the straight fins (Fig. 9), one of the most common extended surfaces, was also modeled by using the simulator. The temperature distribution on thallium in this case with the water flow rates of 10, 15, 25, 35 and 45 L/min are shown in Fig. 10.

It can be seen from these results that the maximum temperature of thallium on the target with fins and the water flow rate of 10 L/min is 463 K, whereas the maximum temperature of thallium on the target without fins is 583 K that is more than thallium melting point. Therefore, it can be concluded that within the same irradiation parameters, the target with fins needs cooling water at a lower flow rate to reach the same temperature.

Conclusions

Since the increasing of the beam current in an irradiation process is resulting in a higher radionuclide production and decreasing the irradiation time as a result, so there are always trials to irradiate a target with a maximum beam current. But, with increasing beam current the heat generated in the target is increased and the target temperature goes up. Therefore, one of the important issues in designing a targetry system is heat transfer and control of target temperature during irradiation.

In this study, the basic equations were used for modeling of heat transfer in a solid target for the production of ²⁰¹Tl by using a simulator of SolidWorks®2010. The thermal distributions have been simulated within the different practical parameters of irradiation

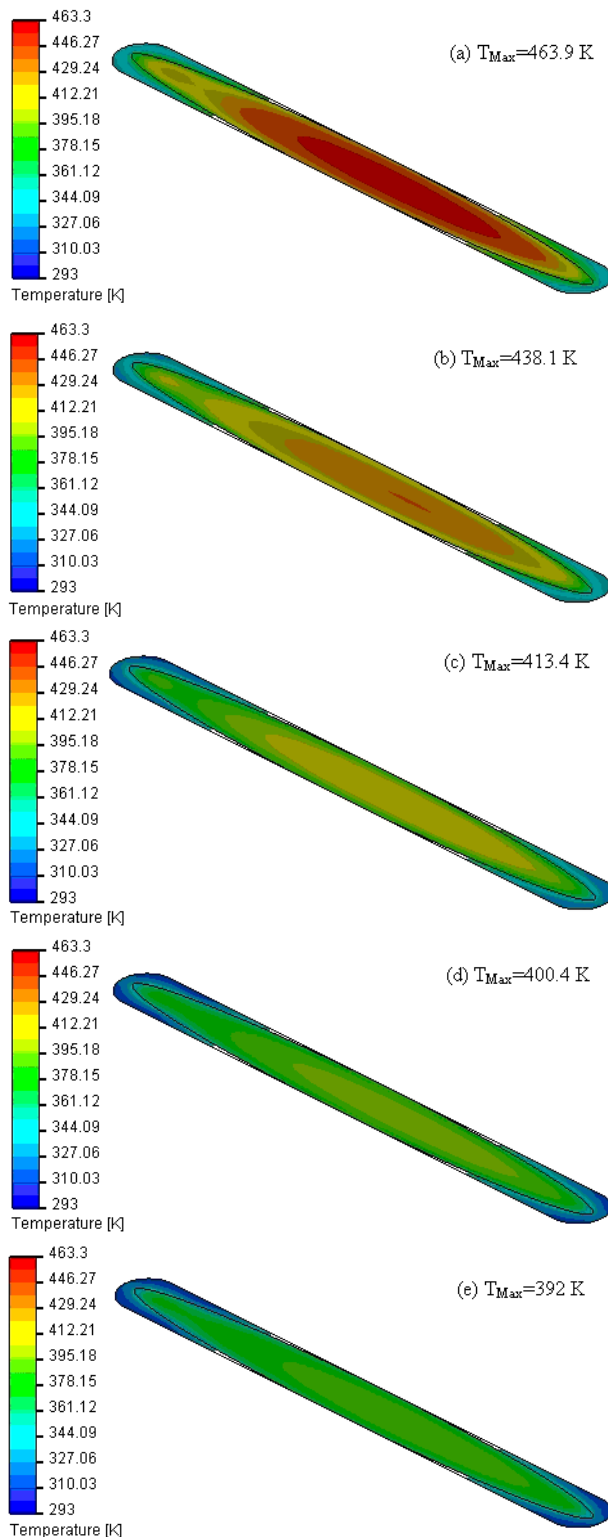


Fig. 10. The modeled thallium temperature distribution on the copper backing with straight fins in the cooling water ($T_{\text{water}} = 293 \text{ K}$) at flow rates of (a) 10 L/min ($Re = 21\ 335$), (b) 15 L/min ($Re = 31\ 032$), (c) 25 L/min ($Re = 56\ 246$), (d) 35 L/min ($Re = 77\ 580$) and (e) 45 L/min ($Re = 100\ 855$).

of the target. From the results of this study it can be concluded that:

1. With an increase of beam current, the maximum temperature of target increases linearly. The current can be increased up to 350 μA and cooling water flow rate be brought down to 15 L/min while the

temperature of the target is still under its melting point.

2. The maximum temperature of target in fined-target system is less than the target system without fins.
3. A slight curve in water flow direction in the inlet of cooling channel can help to increase the water velocity which would result in the temperature homogeneity of the target surface.

By application of these results we can potentially expect almost doubled quantities of ^{201}Tl in the same period of irradiation.

References

1. Arpaci VS (1966) Conduction heat transfer. Addison-Wesley Publication Co., Reading Mass, pp 32–60
2. Dadparvar S, Hussain R, Esteves F *et al.* (2002) Thallium-201 imaging in evaluation of Hodgkin's disease. *Cancer J* 8;6:469–475
3. Frater CJ, Murray IP, Rossleigh M (2001) Tl-201 scintigraphy in muscle trauma. *Clin Nucl Med* 26;1:72–73
4. Haas RLM, Valdés-Olmos RA, Hoefnagel CA *et al.* (2003) Thallium-201-chloride scintigraphy in staging and monitoring radiotherapy response in follicular lymphoma patients. *Radiother Oncol* 69;3:323–328
5. Hardoff R, Baron E, Sheinfeld M (1991) Early and late lesion-to-non lesion ratio of Tl-201-chloride uptake in the evaluation of cold thyroid nodules. *J Nucl Med* 32;10:1873–1876
6. Human GP, Dormehl I (1991) Imaging of the myocardium with thallium-201. *S Afr Med J* 59;15:524–528
7. IAEA (2005) Standardized high current solid targets for cyclotron production of diagnostic and therapeutic radionuclides. STI/DOC/010/432. TECDOC-1412. International Atomic Energy Agency, Vienna
8. Lauer MS (2005) Prediction of the death or myocardial infarction by exercise single proton emission computed tomography perfusion scintigraphy in patients who have recent coronary artery stenting. *Am Heart J* 149;3:534–540
9. Lide DR (ed) (2004) Handbook of chemistry and physics, 84th ed. CRC Press, Boca Raton
10. Lin CC, Ding HJ, Chen YW, Huang WT, Kao A (2004) Usefulness of thallium-201 muscle perfusion scan to investigate perfusion reserve in the lower limbs of type 2 diabetic patients. *J Diabetes Complications* 18;4:233–236
11. Perry RH, Green DW (eds) (1997) Perry's chemical engineers' handbook, 7th ed. McGraw-Hill, New York
12. Sehweil AM, McKillop JH, Milroy R, Wilson R, Abdel-Dayem HM, Omar YT (1989) Mechanism of ^{201}Tl uptake in tumors. *Eur J Nucl Med* 15;7:376–379
13. Sudo Y, Miyata K, Ikawa H, Kaminga M, Ohkawara M (1985) Experimental study of differences in DNB heat flux between upflow and downflow in vertical rectangular channel. *J Nucl Sci Technol* 22:604–618
14. Ziegler JF, Biersack JP, Littmark U (1985) The stopping and range of ions in solids. Pergamon Press, New York